Free growth of a thermotropic columnar mesophase : supersaturation effects

P. Oswald, J. Malthête, P. Pelcé

Classification
Physics Abstracts
61.30 — 68.70

Free growth of a thermotropic columnar mesophase : supersaturation effects

P. Oswald ([1]), J. Malthête ([2]) and P. Pelcé ([3])

([1]) Laboratoire de Physique de l'Ecole Normale Supérieure de Lyon, 46 Allée d'Italie, 69364 Lyon Cedex 07, France

([2]) Laboratoire de Chimie de l'Ecole Normale Supérieure de Lyon, 46 Allée d'Italie, 69364 Lyon Cedex 07, France

([3]) Laboratoire de Recherche en Combustion, Université de Provence-St Jerome, 13397 Marseille Cedex 13, France

(*Reçu le 21 mars 1989, accepté le 25 avril 1989*)

Résumé. — Nous décrivons la croissance libre (à température constante) d'un cristal liquide colonnaire hexagonal. Le matériau choisi est l'hexaoctyloxytriphénylène. Nous observons trois régimes de croissance suivant la valeur de la sursaturation Δ : un régime « pétale » pour $\Delta < 0{,}2$, un régime dendritique pour $0{,}2 < \Delta < 0{,}6$ et un régime de branchements denses pour $\Delta > 0{,}6$. La première transition est expliquée dans le cadre du modèle de Brener *et al.* [6] par un effet de confinement et de nombre Péclet fini. La seconde transition morphologique reste pour l'instant inexpliquée.

Abstract. — The free growth (at constant temperature) of a columnar hexagonal liquid crystal is described. The chosen material is the hexaoctyloxytriphenylene. Three growth regimes are observed depending upon the value of the supersaturation Δ : a petal-shape regime for $\Delta < 0.2$, a dendritic regime for $0.2 < \Delta < 0.6$ and a dense branching regime for $\Delta > 0.6$. The first morphological transition is explained in the framework of the model of Brener *et al.* [6] by an effect of confinement and finite Peclet number. The second morphological transition remains unexplained for the moment.

1. Introduction.

The growth of a solid (an alloy most of the time) in a liquid which is cooled below its solidification temperature leads very often to the formation of dendrites. These dendrites are very important in practice because they are responsible for the solute segregation and thus, for the microstructure of the alloy. These data are essential in metallurgy because they strongly affect the hot ductibility of the material as well as its corrosion resistance, toughness or strength.

Materials which are usually studied are metals or plastic crystals (pivalic acid, succinonitrile). The latter ones have the advantage to be transparent and to melt at low temperatures.

Recently we have shown that it was possible to make grow dendrites in more complex systems such as columnar or smectic liquid crystals [1, 2].

Liquid crystals are interesting for many reasons. They are transparent (and birefringent most of the time) and melt at low temperature. On the other hand, their physical constants (latent heat, surface tension, anisotropy, diffusivity, etc.) are very different from classical materials. So they are very good candidates for testing theoretical scaling laws.

An important problem is the understanding of the different morphologies observed during the growth of a single crystal from a supersaturated solution as a function of the supersaturation and how the transition between these different morphologies occurs. For this study, we have chosen a well known columnar liquid crystal, the 2, 3, 6, 7, 10, 11-hexa-*n* - octyloxytriphenylene (HET in the following) [3]. Many of its physical constants have been measured and some particular aspects of its growth have already been published. Let us mention a study of the initial destabilization of a circular germ and of its weakly non linear evolution [4] and a measurement of the stability constant of a free dendrite [1].

In this article, we sum up in a more complete way these results by including supersaturation effects. We show the existence of three distinct regimes of growth, namely : the petal-shape regime at very small undercooling (or supersaturation), the dendritic regime at intermediate supersaturations and a dense-branching regime at large supersaturation. In each case the shape and the compacity of the monodomain are very different. We shall describe these three regimes of growth in three distinct paragraphs (Sects. 4, 5 and 6). In the following section (Sect. 2) we recall the experimental procedure and its difficulties. In section 3 we discuss qualitatively the theoretical aspects of the problem.

2. Experimental.

HET has been synthetized by one of us (J.M.). This disc-like molecule (Fig. 1a) exhibits an hexagonal columnar phase (Fig. 1b) between 67 and 84.4 °C and is an isotropic liquid above 84.4 °C. The latent heat of the hexagonal-isotropic transition is $L = 1$ kcal/mole [3]. The phase diagram of HET in the presence of a small amount of impurities can be found in

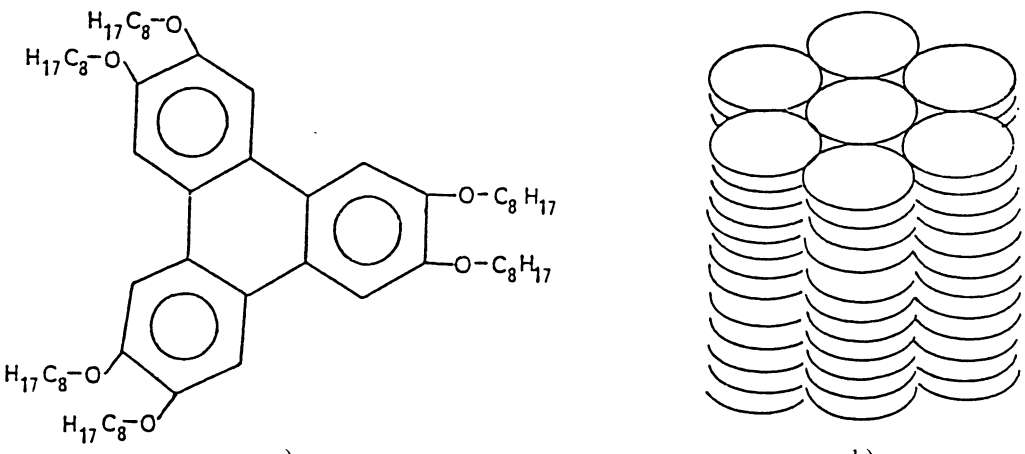

a) b)

Fig. 1. — a) Hexaoctyloxytriphenylene. b) Hexagonal columnar phase. The disc like molecules pack in long parallel columns forming an hexagonal array.

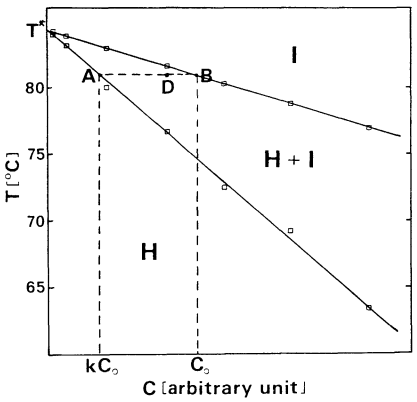

Fig. 2. — Phase diagram (from Ref. [1]).

reference [1]. Both liquidus and solidus are straight lines (Fig. 2). The partition coefficient k of the impurities (defined to be the ratio of the slope of the liquidus to the one of the solidus) is of the order of 0.35 ± 0.03. This apparently large value is due to the fact that we have a liquid crystal and not a solid phase. The diffusion coefficient D of the impurities in the liquid has been measured in directional solidification [5] : $D \sim 1.2 \times 10^{-7}$ cm^2/s. The samples are prepared between two parallel glass plates. Their thickness never exceeds 5 μm. They are placed into a hot stage whose temperature is controlled to about ± 0.02 °C. A polarizing microscope is used for optical observations. We observed that very thin samples orient spontaneously with the molecular columns normal to the glass surfaces. In the following, we shall only describe the growth in the basal plane i.e. the one of the hexagonal lattice. In this plane, the interface is rough and the anisotropy of the surface tension is close to 0.1 [1]. The isotropic-hexagonal surface tension has also been measured : $\gamma \sim 0.52$ erg/cm^2. We can then calculate the typical length $\gamma/L \sim 1.2$ Å. We also measured the liquidus and solidus temperatures for our sample : $T_{\text{liq.}} \sim 82.4$ °C and $T_{\text{sol.}} \sim 78.5$ °C. The control parameter is the undercooling $\Delta T = T_{\text{liq.}} - T$ or equivalently the supersaturation Δ which is a dimensionless parameter defined to be (Fig. 2) :

$$\Delta = BC/AC = \Delta T/mC_0(k-1) = \Delta T/(mC_\infty - \Delta T)(k-1) \qquad (1)$$

This parameter varies from 0 to 1. m is the slope of the liquidus (negative in our case). C_0 is the impurity concentration in the liquid nearby the interface assumed to be flat and C_∞ the mean concentration of impurity in the sample. Experimentally these parameters are difficult to measure very accurately for many reasons : lack of homogeneity of the impurity concentration, slow chemical shift of the sample because of its degradation at high temperature, slight temperature gradient (less than 0.1 °C) between the middle of the sample and its sides... An other convenient method to measure Δ is to wait until the system reaches its thermodynamic equilibrium. In this limit, $\Delta = x$ where x is the volume fraction of cristallized material. This method requires a time at least equal to ℓ^2/D where ℓ is the average distance between germs and so, is applicable for large enough values of the supersaturation ($\Delta > 0.2$). We shall see in the following that it is also possible to estimate Δ from the evolution in time of the area of the germ. Finally, let us notice an important limitation of this experiment related to boundary and neighbour effects. These effects appear when the distance between a germ and the sample sides (or an other germ) is of the same order as the

diffusion length $\ell_d = 2\,D/V$ where V is the growth rate. At small supersaturation ($\Delta < 0.2$), the main limitation stems from the finite size of the sample (1 cm^2 in our experiment). At higher supersaturation, the nucleation rate of new germs becomes important and the interactions between neighbours are quickly cumbersome. Nevertheless, the diffusion length is the more small as Δ is large which limits the effects of the confinement. In practice we can disregard them up to a certain size of the domain which can vary with the supersaturation but never exceeds a few hundreds of μm.

3. Theoretical aspects of the problem.

In order to understand these morphologies, we need three theoretical features that we expose in the following :

a. THE FINITE SIZE EFFECTS. — We assume that the medium is two-dimensional since the thickness of the sample is much smaller than its lateral dimensions L. Let us assume that n germs are initially present in the system and that the initial concentration is C_∞. Let C_0 be the equilibrium concentration on the liquidus line corresponding to the temperature of the sample. Let R be the final radius of a germ. The conservation of impurities implies that

$$c_\infty L^2 = n\pi R^2 K c_0 + c_0(L^2 - n\pi R^2) \tag{2}$$

or that

$$\Delta = n\pi R^2/L^2 . \tag{3}$$

b. THE MULLINS-SEKERKA INSTABILITY. — A growing circular germ is unstable with respect to the Mullins-Sekerka instability. The growth rate of the instability can be written as

$$\omega_j = \frac{j-1}{R_0}\frac{\mathrm{d}R_0}{\mathrm{d}t}\left(1 - \frac{j(j+1)\,d_0\,D_L}{R_0^2\dfrac{\mathrm{d}R_0}{\mathrm{d}t}}\right). \tag{4}$$

Here the radius of the germ is slightly deformed as :

$$R(t) = R_0(t) + \delta_j \exp(\omega_j t)\cos j\theta \tag{5}$$

where θ is the polar angle. d_0 is the capillary length defined as $d_0 = (\gamma/L)(T^*/mC_0(k-1))$ in the chemical case. The expression for the growth rate is valid in the quasistationary approximation, i.e. when it is much larger than the inverse of the time scale for the evolution of the radius R_0. In the limit R_0 goes to $+\infty$, j goes to $+\infty$, $j/R_0 = k$, one obtains the usual Mullins-Sekerka growth rate as

$$\omega = Vk\left(1 - d_0\frac{D}{V}k^2\right) \tag{6}$$

where $V = \mathrm{d}R_0/\mathrm{d}t$. The largest growth rate is obtained for the most unstable wavelength $\lambda_c = 2\,\pi\,(3\,d_0\,D/V)^{1/2}$.

c. CRYSTAL GROWTH IN A CHANNEL. — When the circular germ becomes unstable, a six fold periodic structure is generated so that each petal can be considered as a single crystal growing in a divergent capillary. Crystal growth in a capillary of uniform section is now well understood. Let us introduce the dimensionless diameter $\Lambda = \ell/d_0$ where ℓ is the width of the

capillary and d_0 the capillary length. In a recent study, Brenner *et al.* [6] determine approximate solutions for needle crystals growing at constant velocity. For a given undercooling the growth rate appears as a two-valued function of the diameter Λ when this diameter is larger than a critical value $\Lambda_c(\Delta)$. Three of these curves are shown in figure 3 for the values of Δ equal to 0.1 ; 0.2 and 0.3 and a surface tension anisotropy β equal to 0.1. It appears that $\Lambda_c(\Delta)$ is a rapidly decreasing function of Δ. The lower branch is at low Peclet number (defined to be Pe = $\ell V/2D$), and corresponds to the Saffman-Taylor branch already discussed by many authors [7, 9]. As shown analytically, [10] this branch is unstable with respect to tip-widening instability, which is confirmed by experiments [11] and numerical simulations [12]. The upper branch, at Peclet number larger than 1, is stable and corresponds to free dendritic growth when Λ goes to infinity. When Λ is smaller than $\Lambda_c(\Delta)$, the growth is not stationary.

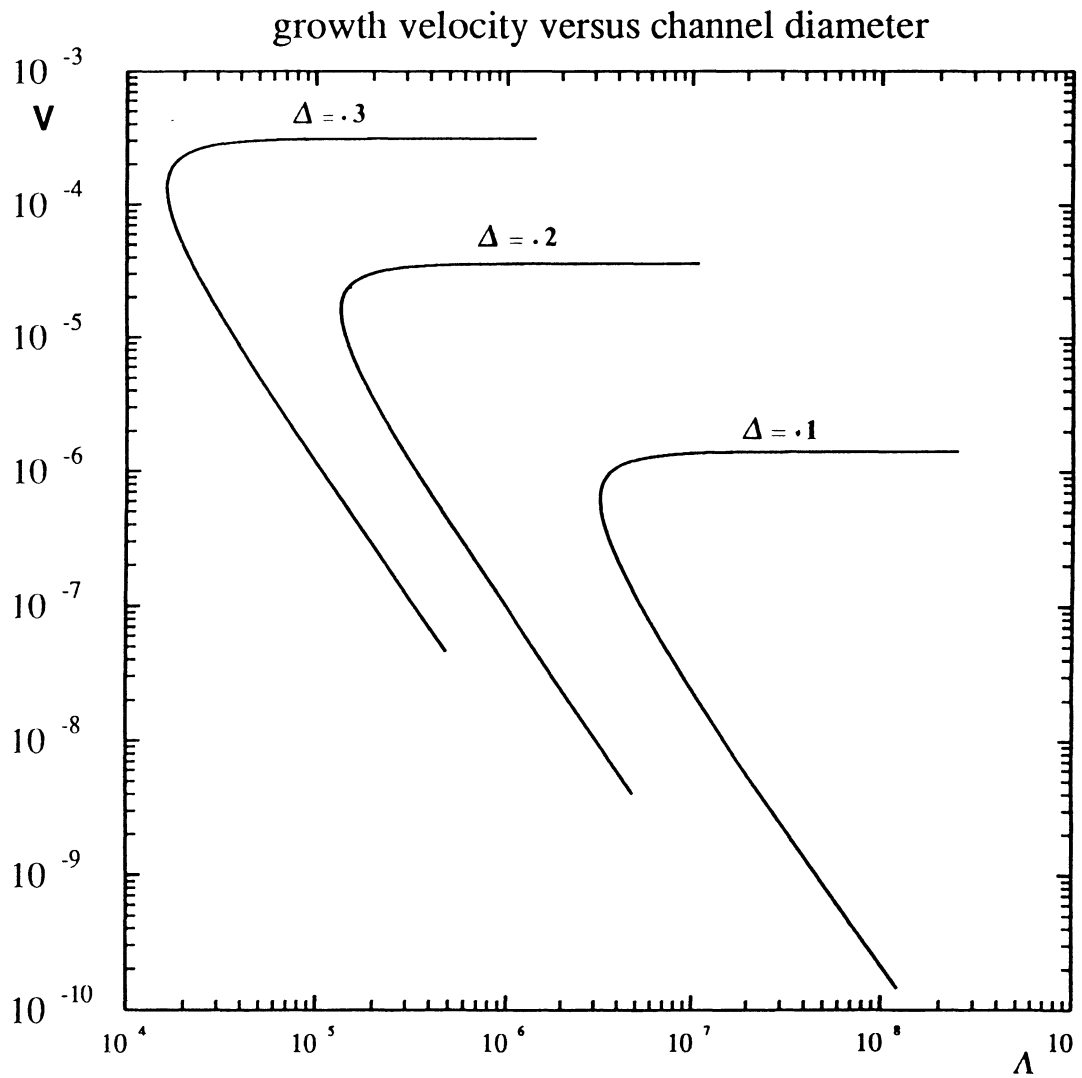

Fig. 3. — Dimensionless growth velocity (in unit $2D/d_0$) *versus* channel diameter (adapted from Fig. 3a of Ref. [6] for Δ = 0.1 ; 0.2 ; 0.3 and β = 0.1).

4. The petal shape regime.

It is observed at small supersaturation, typically $\Delta < 0.2$. We already described this growth regime in a previous article [4] (Fig. 4). In this section we summarize the main results already obtained :

— the germ, circular at the beginning, destabilizes above a certain radius R_6 : an hexagonal modulation develops which is amplified by the destabilizing effect of the diffusion field. A linear stability analysis (Mullins-Sekerka theory) gives R_6 as a function of the capillary length d_0. Comparison between theory and experiment gives $d_0 \sim 200$ Å. This value is in good agreement with the one we can directly calculate from the phase diagram ;

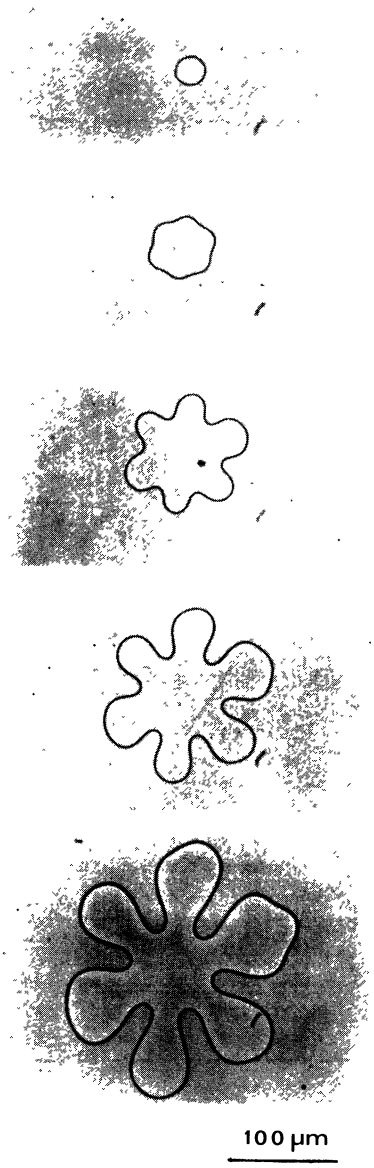

Fig. 4. — Petal-shape regime ($\Delta = 0.15$).

— a harmonic analysis of the shape of the germ shows that the 12th and 18th modes are both in phase opposition with the 6th mode (Fig. 5a). They correspond to a non linear saturation of the hexagonal mode and should lead to a tip-splitting instability of each branch of the monodomain. Because of the confinement and of the slowing down of the growth at long time, we did not observe this second instability ;

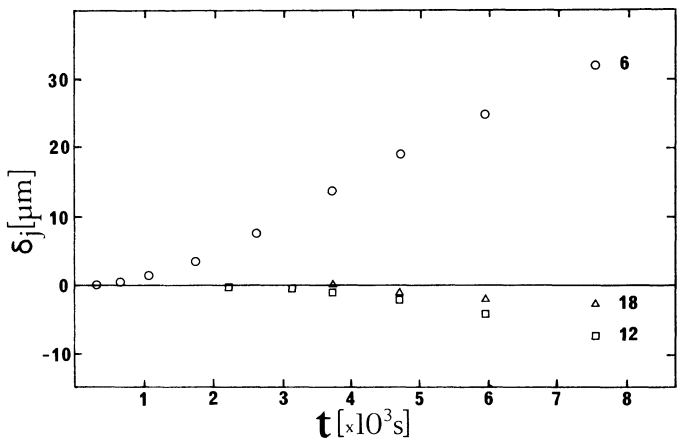

a)

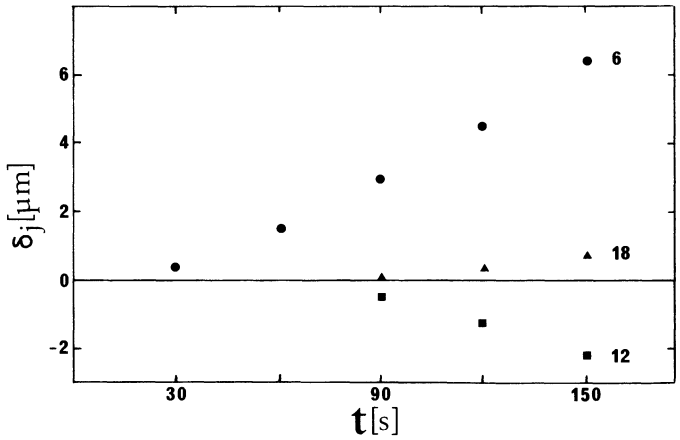

b)

Fig. 5. — Experimental Fourier component δ_j *versus* time in the weakly non linear regime (see Eq. (4)). The value of j is indicated on each curve. a) $\Delta = 0.1$ (petal shape regime ; from Ref. [4]) ; b) $\Delta = 0.3$ (dendritic regime).

— the total area A of the germ increases linearly in time (Fig. 6a) as long as boundary effects are negligible. This result is compatible with the numerical simulations of Brush [13]. As was shown by this author, the linear dependence of the area *versus* time remains valid in the non linear regime (whatever the shape of the germ) if the Peclet number defined to be $Pe = RV/2D$ is small (R is the radius of the germ) and if the tip radius of each branch is

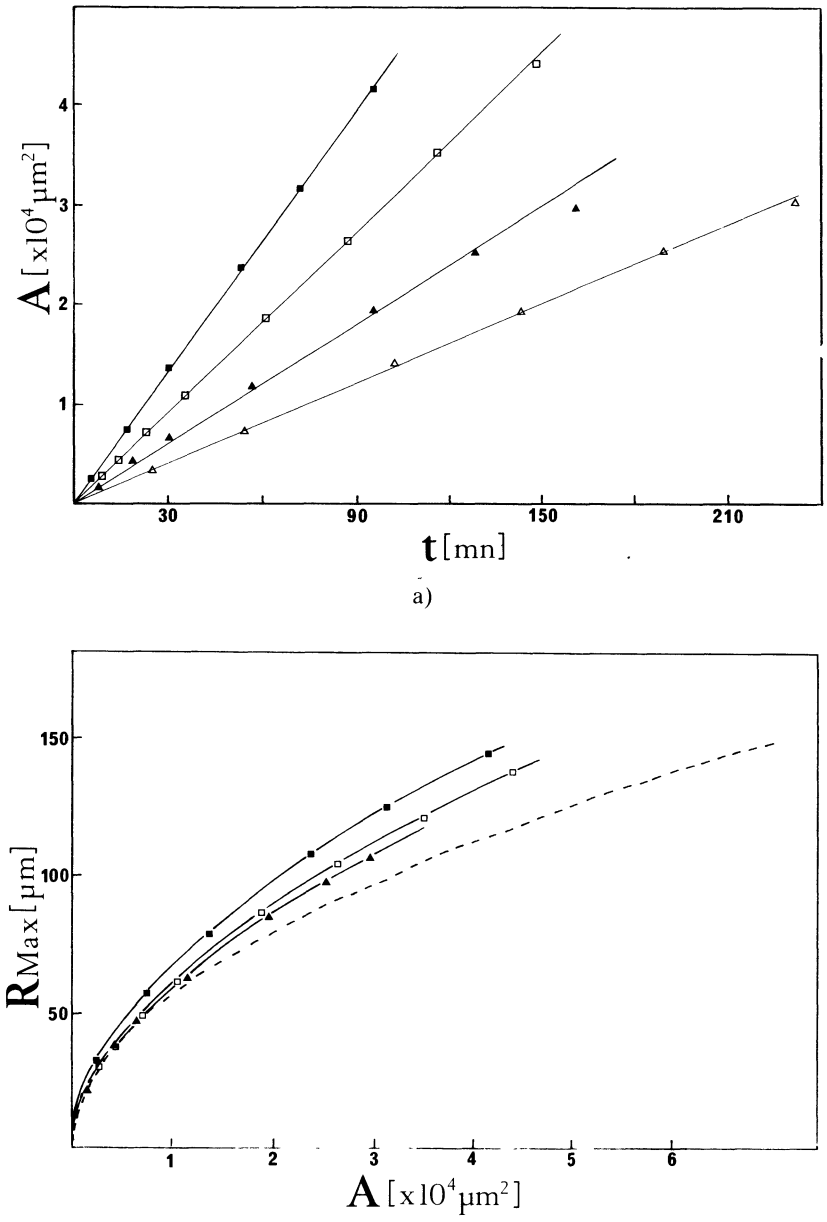

Fig. 6. — Global properties of a germ in the petal shape regime ; a) total area *versus* time ; b) maximum radius of the germ *versus* its area (the dotted line corresponds to a circular germ).

sufficiently large compared to the capillary length. Thus, the variation of the total area can be computed by assuming that the germ is circular and by using the well known self-similar solution in $t^{1/2}$. The measurement of the slope of $A(t)$ enables us to calculate the supersaturation Δ. Remember that

$$dA/dt = 4\,\pi D\lambda^{2} \tag{7}$$

where λ^2 is a function of Δ which is given by [14] :

$$\lambda^2 \exp \lambda^2 \mathrm{Ei}\ (-\lambda^2) + \Delta = 0 \tag{8}$$

Ei (x) is the exponential integral function;

— the maximum radius of the germ increases as $t^{1/2}$, as can be seen in figure 6b even in the non linear regime. In this figure, we plotted $R_{\mathrm{Max.}}$ *versus* the area A of the germ for various values of the sursaturation Δ (calculated from the measured slope $\mathrm{d}A/\mathrm{d}t$ *via* Eqs. (7) and (8)). In this regime the radius of curvature of the tip of each branch continuously increases whereas the tip velocity decreases as $t^{-1/2}$. This result is essential. It characterizes this time-dependent growth regime.

5. The dendritic regime.

For values of the supersaturation lying between 0.2 and 0.6, we observe another type of growth. The destabilization mechanism is always the same at the beginning and the hexagonal mode first develops. Its non linear evolution is however quite different because each branch leads very quickly to a dendrite. Figure 7 shows the typical evolution of a germ at $\Delta \sim 0.3$. In this sequence, the sidebranching is not very developed. By increasing Δ, the sidebranching develops, leading to more and more compact germs (Fig. 8). Note in figure 7c that the germ is almost circular : the six primary dendrites are still visible. Their tips are stable but their secondary branches are unstable wih respect to tip-splitting instability. By further increasing the supersaturation, the tips of the primary dendrites become themselves unstable by tip-splitting instability. It is then impossible to recognize any direction of privileged growth. This regime will be described in the next section. We made again a global analysis of the germ for various supersaturations. Then we were interested in the local properties of a dendrite (velocity and radius of curvature of its tip).

5.1 GLOBAL PROPERTIES. — We made again a harmonic analysis of the shape of the germ just after its destabilization (Fig. 5b). One observes that the first mode to appear is still the hexagonal one. The following one is the 12th mode still in phase opposition with the 6th. The 18th mode then appears. Contrary to the petal-shape regime, this mode is in phase with the fundamental one. It seems to us that the further evolution of the germ is tightly related to the sign of this mode. It is also worth noting that this mode corresponds to the development of a side-branching instability.

We also measured the area of the germ against time for many supersaturations (Fig. 9a). In every case, $A(t)$ is a linear function. This is a consequence of the impurity conservation. The values of Δ, obtained by direct measurement of the undercooling, or by measurement of the volumic fraction x of hexagonal phase at equilibrium, are in good agreement with the one we deduce from the slope $\mathrm{d}A/\mathrm{d}t$ *via* equations (7) and (8). These results are compared in table I.

Table I.

ΔT (± 0.05 °C)	Δ (Phase diagram)	Δ (slope $\mathrm{d}A/\mathrm{d}t$)	x
0.1	0.037-0.106	0.1	—
0.4	0.226-0.278	0.26	—
0.45	0.253-0.303	0.29	0.27
0.7	0.370-0.410	0.45	0.42
2.2	0.785-0.800	—	0.82

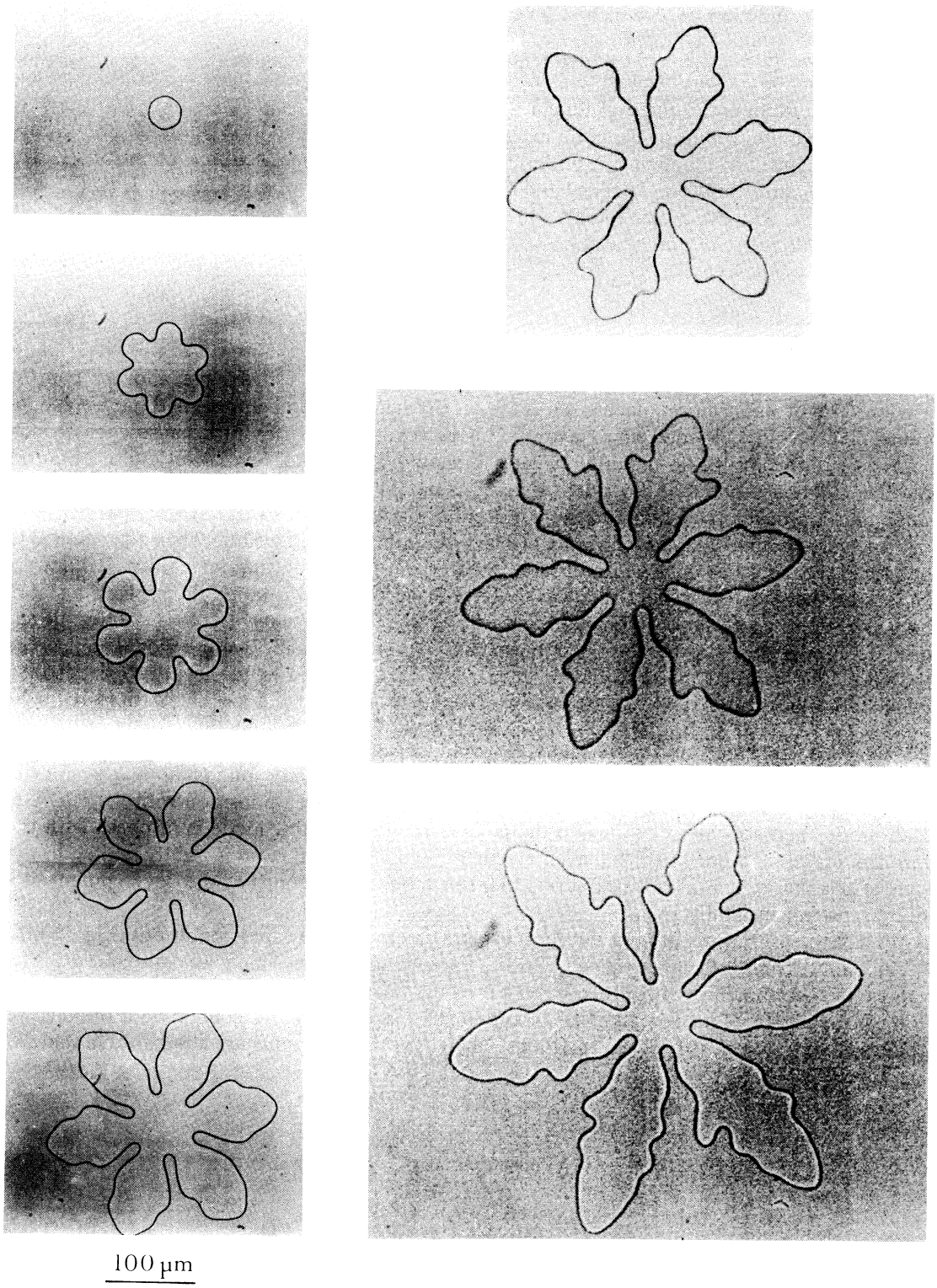

Fig. 7. — Dendritic regime ($\Delta = 0.3$).

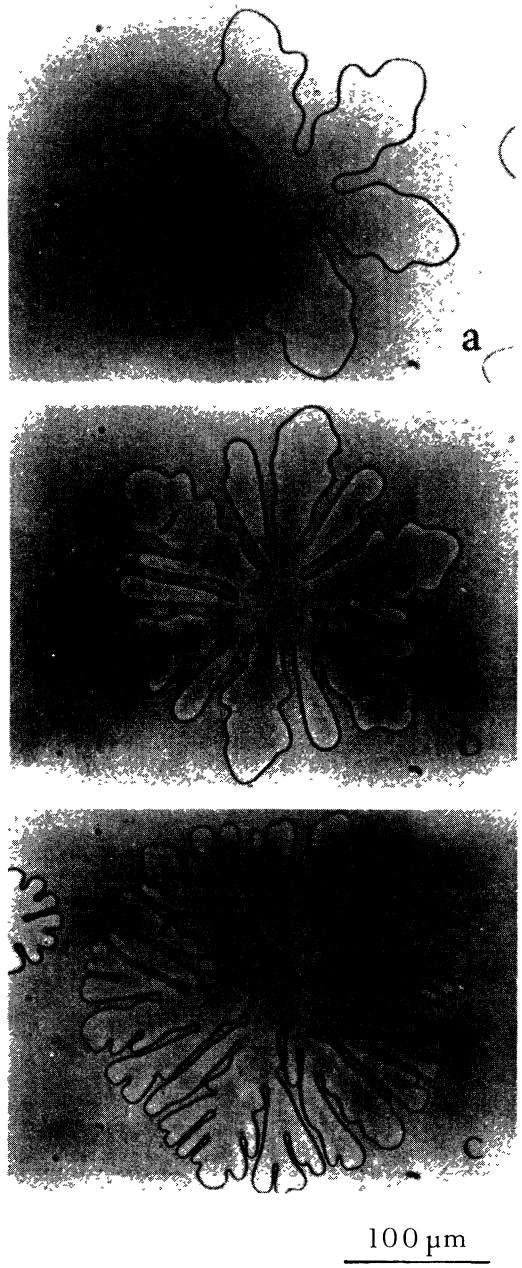

Fig. 8. — Germs in the dendritic regime at various supersaturations ; a) $\Delta = 0.24$; b) $\Delta = 0.45$; c) $\Delta = 0.63$.

Finally we plotted $R_{\text{Max.}}$ *versus* A (proportional to t) (Fig. 9b). All these curves are similar (within the experimental error) and superimpose. One observes two behaviours : a transient regime during which $R_{\text{Max.}}$ increases as $A^{1/2}$ (or $t^{1/2}$) followed by a permanent one during which $R_{\text{Max.}}$ is a linear function of A (or t). In this limit the six dendrites are independent : their tips have a constant curvature and move at constant velocity $V = \mathrm{d}R_{\text{Max.}}/\mathrm{d}t$.

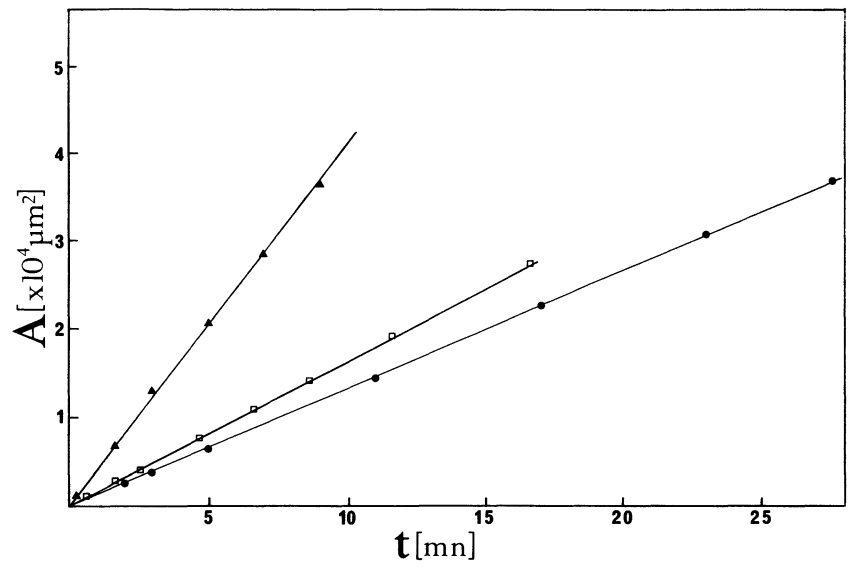

a)

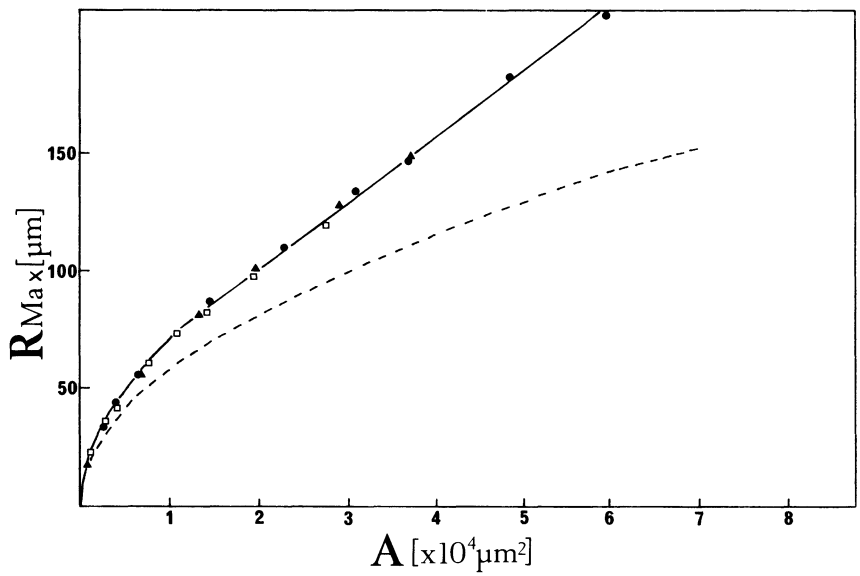

b)

Fig. 9. — Global properties of a germ in the dendritic regime ; a) total area *versus* time ; b) maximum radius of the germ *versus* its area (the dotted line corresponds to a circular germ).

These free dendrites belong to a class of stationary solutions which have been already extensively studied both experimentally and theoretically [15, 9]. We summarize their properties (partially published in Ref. [1]) in the next subsection.

5.2 LOCAL PROPERTIES OF A DENDRITE. — For each dendrite we measured the velocity V and the radius of curvature ρ of its tip. Such a measurement is difficult because it requires to wait until the dendrite gets its stationary growth regime. In figure 10 we plotted Ln ρ as a function of Ln V for various supersaturations. We found a linear law : its slope is near to 0.45 which means the velocity is approximately proportional to the square of the curvature. In this experiment $\langle \rho^2 V \rangle \sim 12\ \mu m^3/s$. This law is very robust and is well verified even if the germ is not strictly in a stationary growth regime. This experimental result is compatible with the theory and the selection mechanism by surface tension anisotropy (see

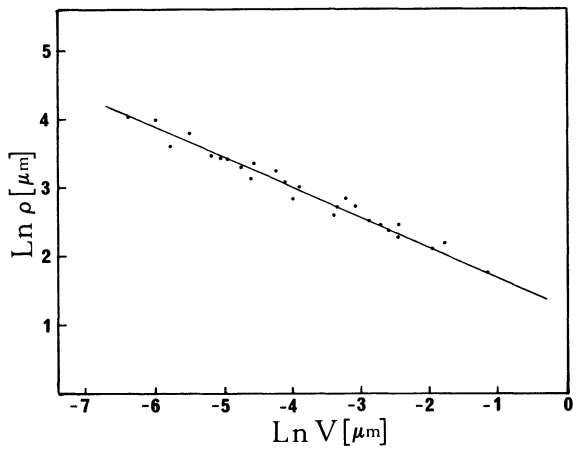

Fig. 10. — Dendrite tip radius against tip velocity. These measurements have been made on different dendrites at various supersaturations.

Ref. [1] for further information). It expresses that the radius of curvature is proportional to the most unstable wavelength of the planar front ($\rho \propto \lambda_c \propto (d_0 D/V)^{1/2}$). We also tried to test on a few examples whether the Ivantsov relation was well satisfied. This relation relates the product ρV to the supersaturation Δ. (Such a verification is tricky because one have to make sure that the dendrites are independent and grow at constant velocity.) Table II gives a few values of the Peclet number measured experimentally and calculated from the Ivantsov relation :

$$\Delta = 2\,\mathrm{Pe}^{1/2} \exp \mathrm{Pe} \int_{\mathrm{Pe}^{1/2}}^{\infty} \exp(-y^2)\,dy\,. \tag{9}$$

Remember that the Peclet number is defined to be $\mathrm{Pe} = \rho V/2D$ for a dendrite.

Table II.

Δ	Pe (exp.)	Pe (theory)
0.15	0.011	0.0088
0.2	0.019	0.016
0.25	0.030	0.027
0.29	0.035	0.040
0.45 *	0.069	0.127

* For this value of the supersaturation it is impossible to obtain isolated dendrites.

The agreement between theory and experiment is satisfying according to the fact that the Peclet number varies very fast with the supersaturation Δ.

Let us notice a last original aspect of the growth of this phase. It happens (this is very scarce) that a disclination line pierces the germ. For some reasons of symmetry, this line is necessarily aligned along a two-fold axis of the hexagonal lattice [16] which is also a preferential direction of growth of the dendrites. Figure 11a shows a dendrite whose growth axis is confused with the disclination. It is clear on this picture that this peculiar dendrite is sharper and moves faster than an ordinary dendrite. The defect, whose topology is described in figure 11b, creates a local cusp-like perturbation on the tip which strongly modifies the selection mechanism of this dendrite. A naive interpretation would consist to say that the defect increases the surface tension anisotropy nearby the tip, which leads, according to the theory, to both a sharper and faster dendrite ($\rho^2 V$ decreases whereas ρV remains constant).

Let us discuss now the transition between petal shape and dendritic regimes. As mentionned before, each petal can be considered as a single crystal growing in a divergent capillary with an angle $\theta = 2\pi/6$. We assume that the growth characteristics are similar in a

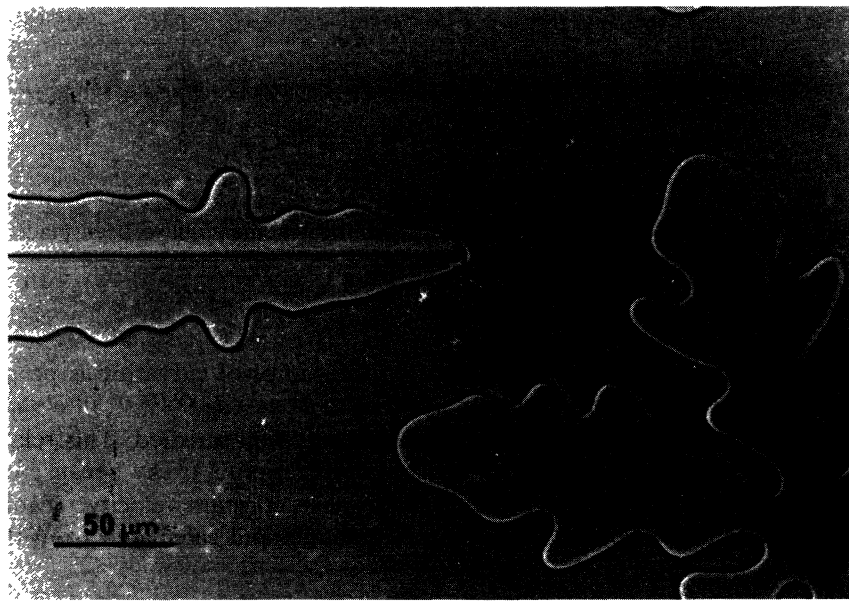

a)

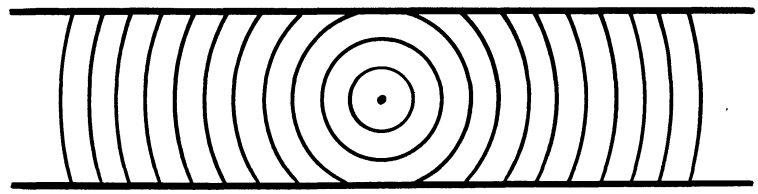

b)

Fig. 11. — a) Anomalous dendrite which is growing along a disclination line : this dendrite is sharper and move faster than the other dendrites. b) Columns configuration in a vertical plane normal to the defect line (schematic).

divergent capillary and in a rectilinear channel, for which theoretical results are available. At least for small angle of divergence, one can approximate the dimensionless channel width $\Lambda = \ell/d_0$ by $2\,\pi R_{\text{Max.}}/6\,d_0$ where $R_{\text{Max.}}$ is the radius of the envelop of the petal tips. As mentionned in section 3c, growth at constant velocity is possible only if Λ is larger than a critical value $\Lambda_c(\Delta)$, a decreasing function of the undercooling. At low undercooling, the final radius R_f of the germ given in section 3a is such as $\Lambda_f = 2\,\pi R_f/6\,d_0$ is smaller than $\Lambda_c(\Delta)$ and unsteady growth is observed (petal shape regime). At larger undercooling the final radius of the germ is larger and $\Lambda_c(\Delta)$ smaller, so that above some critical value Δ_c, for which $\Lambda_c(\Delta)$ and Λ_f are equal, growth at constant velocity, i.e. the dendritic regime, is expected. This is what we observe experimentally. Consider the case $\Delta = 0.3$ for which $\Lambda_c \approx 10^4$ (Fig. 3). As $d_0 = 200$ Å, the size of the corresponding channel is $\ell = 200$ μm. This is of the same order of magnitude as what we observe experimentally at this supersaturation. Despite this good qualitative agreement, further theoretical results are needed to make a quantitative comparison with our experiment. In particular calculations in the divergent geometry remain to be done.

It is interesting to discuss this transition in comparison to what occurs in the viscous fingering problem. In this last problem, the transition between petal-shape and dendritic regimes is observed when a petal meets a small air bubble [17]. In this case the transition is interpreted as being due to the anisotropy of the surface tension induced by the bubble. Similar phenomenon occurs when a thin wire is stretched along the axis of a divergent cell [19] : in this case, anomalous fingers can develop too. Here again, the wire may introduce an anisotropy in the surface tension and allow the growth of fingers of relative width less than 1/2 i.e. fingers scaled with their own tip radius as it is the case for a dendrite. However, differences exist between viscous fingering and crystal growth because of Peclet number effects. This can be simply observed in a rectilinear geometry. In the Saffman-Taylor problem, linearly stable steady states growing with constant velocity exist whatever the driving force. The presence of anisotropic surface tension is not necessary and only changes the allowed values for the growth velocities. In crystal growth, steady states exist only for sufficiently large undercooling. The steady state branch is two valued. Only the upper branch, corresponding to dendritic growth is stable. Thus, transition between unsteady behaviour and growth at constant velocity can be induced by increasing the supersaturation.

6. The dense-branching regime.

At large supersaturation ($\Delta > 0.6$), it is impossible to get a stable dendrite because its tip is unstable with respect to tip-splitting instability. In this regime, the germ is very dense and it is often impossible to recognize the axes of dendritic growth (Fig. 12). The germ is globally circular although the front is very unstable with respect to the tip-splitting instability. Because of the huge rate of nucleation of new germs, it is quasi impossible to obtain large domains. It is also very difficult to measure accurately the supersaturation and an evolution in time of the area of the germ because the temperature of the hot stage is not well stabilized just after the cooling of the sample (20 to 30 s are necessary to stabilize the temperature of our system). By tracing concentric circles and by counting how many times a given circle intersects the interface, it is possible to estimate a characteristic size λ of the cells. We found that λ is independent (at about 20 %) of the radius (Fig. 13) and of the order of the most unstable wavelength of the planar front $\lambda_c = 2\,\pi\,(3\,d_0\,D/V)^{1/2}$. In figure 11 for instance, we measure $\lambda \sim 7$ μm and $V \sim 1.2$ μm/s. By taking $d_0 \sim 200$ Å and $D = 1.2 \times 10^{-7}$ cm^2/s we calculate $\lambda_c \sim 5$ μm which is well of the same order of magnitude as λ.

The transition between dendritic regime and dense branching regime is more difficult to

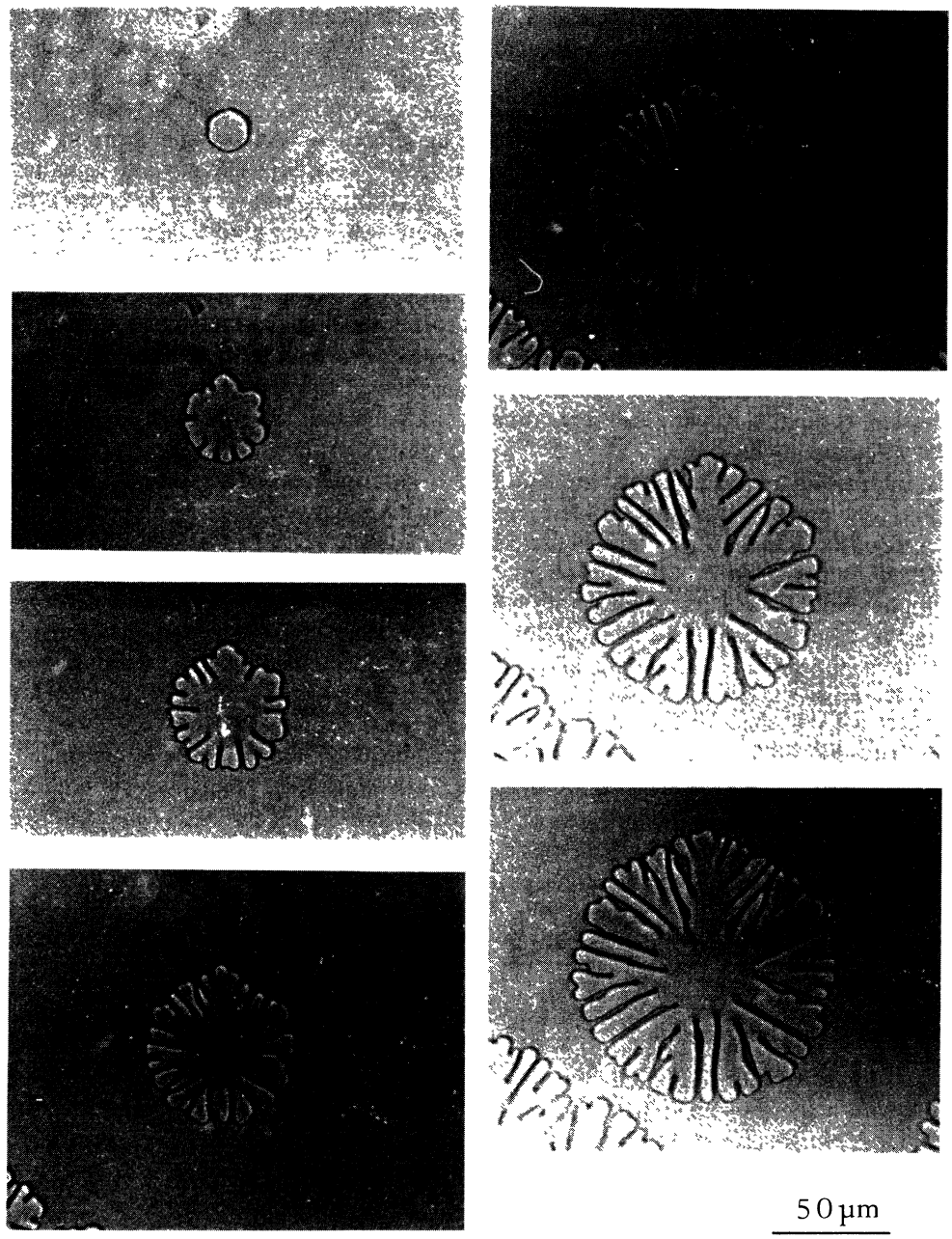

Fig. 12. — Dense branching regime ($\Delta = 0.7$).

explain. From figure 8, it appears that new dendrites are formed with the sidebranching of the six main dendrites. This process appears in directional solidification too. In this case, the wavelength of the dendritic array decreases with the pulling velocity. If this velocity suddenly increases, the reduction of wavelength occurs with the development of the sidebranching of the initial dendrites [18]. The theoretical understanding of this process is not achieved for the moment.

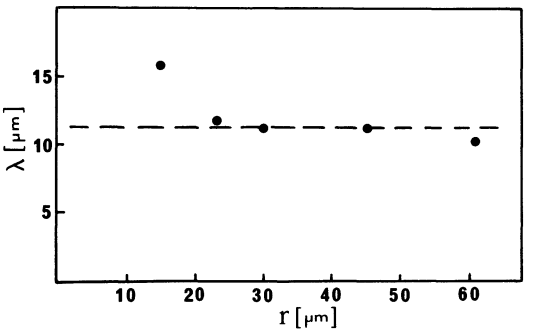

Fig. 13. — Characteristic size λ of the cells *versus* radius r in the dense branching regime.

Concluding remarks.

We observed, described and discussed the different morphologies that a liquid-liquid crystal interface growing from a supersaturated solution can exhibit at different supersaturations.

At low supersaturation, the growth is unsteady, self similar in $\sqrt{t}$. The interface, initially circular, destabilizes to form six petals, whose tip radius grows in $\sqrt{t}$, like the envelope of the germ. At larger supersaturation, each petal destabilizes to form a dendrite, i.e. a single crystal growing with constant velocity. We discuss the transition between the two regimes in connection with the graph « velocity *versus* supersaturation » computed for a crystal growing in a rectilinear channel. At larger velocity a dense branching regime is observed. The reduction of wavelength of the pattern appears to be due to the development of the sidebranching and to the tip-splitting of the six primary dendrites.

Acknowledgments.

One of us (P. O.) would like to thank M. Benamar, V. Hakim and C. Caroli for fruitful discussions. This work was supported by D.R.E.T. contract No. 88/1365.

References

[1] Oswald P., *J. Phys. France* **49** (1988) 1083.
[2] Bechhoefer J., Oswald P. and Libchaber A., *Phys. Rev. A* **37** (1988) 1691.
[3] Destrade C., Moncton M. C. and Malthete J., *J. Phys. Colloq. France* **40** (1979) C3-17.
[4] Oswald P., *J. Phys. France* **49** (1988) 2119.
[5] Oswald P., in *J. Phys. Colloq. France,* **50** (1989) C3-127.
[6] Brener E. A., Gellikman M. B. and Temkin D. E., *Sov. Phys. JETP* **67** (1988) 1003.
[7] Pelce P. and Pumir A., *J. Cryst. Growth* **73** (1985) 337.
[8] Kessler D., Koplik J. and Levine H., *Phys. Rev. A* **34** (1986) 4980.
[9] Pelce P., Dynamics of Curved Fronts (Academic Press) 1988.
[10] Pelce P., *Europhys. Lett.* **7** (1988) 453.
[11] Bechhoeffer J., Guido H. and Libchaber A., *C.R. Acad. Sci. Paris Ser. II* **306** (1988) 619.
[12] Kessler D. and Levine H., preprint (1988).
[13] Brush L. N., Advanced Numerical Methods in Solidification Theory, Phd Thesis 1987.
[14] Coriell S. R., Parker R. L., *J. Appl. Phys.* **36** (1965) 632.

[15] LANGER J. S., Les Houches XLVI, Chance and Matter, Eds. J. Souletie, J. Vannimenus, R. Stora (Elsevier) 1987.
[16] OSWALD P., *J. Phys. Lett. France* **42** (1981) L171.
[17] COUDER Y., CARDOSO O., DUPUY D. and TAVERNIER P., *Europhys. Lett.* **2** (1986) 437.
[18] JACKSON K. A., HUNT J. D., UHLMANN D. R. and SEWARD III T. P., *Trans. A.I.M.E.,* **236** (1966) 149, see also reference [2].
[19] THOME H., RABAUD, M., HAKIM V. and COUDER Y., preprint (1988).